THE JOURNAL OF PHYSICAL CHEMISTRY A

Article

pubs.acs.org/JPCA

Role of the Recombination Channel in the Reaction between the HO and HO_2 Radicals

María P. Badenes,* María E. Tucceri, and Carlos J. Cobos

Instituto de Investigaciones Fisicoquímicas Teóricas y Aplicadas (INIFTA), Departamento de Química, Facultad de Ciencias Exactas, Universidad Nacional de La Plata, CONICET, Casilla de Correo 16, Sucursal 4, 1900 La Plata, Argentina

ABSTRACT: The kinetics of the gas phase recombination reaction HO + HO_2 + He → HOOOH + He has been studied between 200 and 600 K by using the SACM/CT model and the unimolecular rate theory. The molecular properties of HOOOH were derived at the CCSD(T)/aug-cc-pVTZ ab initio level of theory, while relevant potential energy features of the reaction were calculated at the CCSD(T)/aug-cc-pVTZ//CCSD(T)/aug-cc-pVDZ level. The resulting high and low pressure limit rate coefficients are $k_\infty = 3.55 \times 10^{-12} (T/300)^{0.20}$ cm^3 molecule^{-1} s^{-1} and k_0 = [He] $1.55 \times 10^{-31} (T/300)^{-3.2}$ cm^3 molecule^{-1} s^{-1}. The rate coefficients calculated over the 6×10^{-4} − 400 bar range are smaller at least in a factor of about 60 than the consensus value determined for the main reaction channel HO + HO_2 → H_2O + O_2, indicating that the recombination pathway is irrelevant.

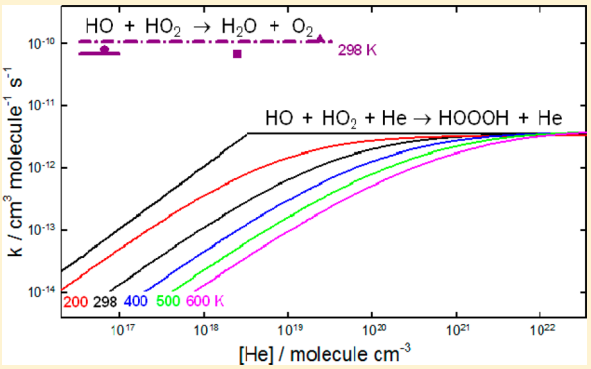

1. INTRODUCTION

The reaction HO + HO_2 → H_2O + O_2 plays a relevant role in atmospheric chemistry. It is a dominant reaction pathway in the removal of the HO and HO_2 radicals, both of which catalytically depletes ozone in the upper atmosphere.[1−3] This is also an important process in combustion chemistry. It is a major consumption process of HO_2 in lean combustion and responsible for the depletion of both radicals in burnt gases.[4,5] In earlier investigations, the recombination reaction via a complex mechanism involving the formation of HOOOH as an intermediate has been proposed.[1,6,7] In this way, two alternative channels were suggested:[1,7]

$$HO + HO_2 \rightarrow H_2O + O_2 \quad (1a)$$

$$HO + HO_2 + M \rightarrow HOOOH + M \quad (1b)$$

Here, M denotes a third-body bath gas and HOOOH the simplest trioxide species for which the synthesis, structural and spectroscopic characterization, and reactivity have been extensively studied and recently reviewed.[7−10] Channel 1a might occur via an energized hydrogen-bonded complex HO−HOO on a triplet potential energy surface, or via the formation of the HOOOH intermediate on a singlet potential energy surface.

Experimental studies of this system suggest pressure dependences between 1 and 1000 Torr, which are not clearly outside the experimental uncertainty and which only may be explained by including reaction 1b in the overall mechanism. The hydrogen-bonded complex is too weakly bonded to generate any important pressure dependence. Because of the interest in this subject, rate coefficients for the present system have been measured by different techniques.[1,5,11] A combination of vacuum UV resonance fluorescence and laser-induced fluorescence (LIF) in a discharge-flow apparatus has been employed to determine the reaction temperature dependence.[1] The rate coefficients have been also measured using a discharge flow reactor and detection by laser magnetic resonance and resonance fluorescence under pseudo first order conditions.[11] The reverse reaction was studied in shock heated $H_2O/O_2/Ar$ mixtures between 1600 and 2200 K employing laser absorption of HO at 306.7 nm and H_2O at 2.5 μm.[5] An extensive report of measured rate coefficients for reaction 1 can be found in refs 4 and 12.

Theoretical studies of the temperature and pressure dependencies of k_{1b} are available. Room temperature falloff curves derived from RRKM calculations based on a totally loose transition state (Gorin model)[13] or using the variational transition state theory with a dipole−dipole potential[14] have been reported. In the last study, it was concluded that the reaction involving HOOOH as an intermediate plays a minor role, except at very high temperatures and/or pressures. In fact, the calculations predict that above 5000 Torr the recombination reaction 1b could compete with the dominant reaction channel 1a. However, the long-range potential employed in these studies probably overestimates the attractive forces between the HO and HO_2 radicals, thus avoiding the region of the potential energy surface where anisotropic effects associated with the transitional modes are operative. As a consequence, the high pressure region of the falloff curves was overestimated. Hence, considerable controversy of the pressure

Received: October 16, 2016
Revised: November 25, 2016
Published: December 22, 2016

DOI: 10.1021/acs.jpca.6b10427
J. Phys. Chem. A 2017, 121, 440−447

effects on the rate coefficients of this reaction still remain. However, nowadays it is possible to characterize the potential energy surfaces using accurate ab initio models. Therefore, to establish the importance of reaction HO + HO_2 + He → HOOOH + He on the global process, a quantum-chemical and kinetic study of this recombination reaction was carried out.

2. COMPUTATIONAL DETAILS

The high correlated coupled cluster singles and doubles excitations approach, including a perturbational estimate of the triples, CCSD(T), was used to fully optimize the molecular structure of the most stable conformation of HOOOH and derive its harmonic vibrational frequencies.[15] The aug-cc-pVTZ Dunning correlation basis set was selected for these calculations.[16]

To employ in the kinetic studies of the HO + HO_2 → HOOOH reaction, electronic potential curves along the minimum energy pathways (MEP) were computed with the G3(MP2)B3,[17,18] G4(MP2),[19] and G4[20] ab initio composite models. In the first two models, the B3LYP/6-311++G-(3df,3pd) functional was used to obtain molecular structures and harmonic vibrational frequencies, whereas in the G4 model the B3LYP/6-31G(2df,p) level was employed. Transitional frequencies along the reaction coordinate were also calculated with the B2PLYP double-hybrid density functional method[21] combined with the 6-311++G(3df,3pd) basis set. In addition, CCSD(T)/aug-cc-pVTZ//CCSD(T)/aug-cc-pVDZ calculations were employed to derive the potential curves. All calculations were performed with the Gaussian 09 package.[22]

Well-established kinetic models of the unimolecular reaction rate theory were used for modeling the HO + HO_2 association reaction. The limiting low pressure rate coefficients k_0 were derived using the strong collision low pressure rate coefficients, k_0^{SC}, estimated with a factorized model.[23,24] The high pressure rate coefficients, k_∞, were calculated with the statistical adiabatic channel model/classical trajectory (SACM/CT) formulation developed for linear rotor + linear rotor type of reactions.[25−27] In addition, the simplified SACM version of refs 28 and 29 was also employed. For the estimation of the pressure dependence of the rate coefficients in the intermediate falloff range, a recently formulated reduced falloff curves method was used.[30,31] In all these calculations, theoretical molecular information provided by the quantum-chemical calculations was employed.

3. RESULTS AND DISCUSSION

3.1. Molecular Structures and Harmonic Vibrational Frequencies. Experimental and theoretical data of the molecular properties of HOOOH have greatly increased in the last years.[32−38] In 2002, Engdahl and Nelander reported a matrix isolation study of HOOOH and presented an infrared spectroscopic identification of this trioxide.[32] However, the first detection in the gas phase was published in 2005 when Endo and co-workers determined its pure rotational spectra and molecular structure.[33] The geometrical structure of HOOOH has been the subject of different experimental and theoretical studies and now it is well-known.[33−38] The CCSD(T)/aug-cc-pVTZ equilibrium structure here calculated is shown in Figure 1. This corresponds to the most stable *trans*-isomer of HOOOH with a zigzag skew-chain and the calculated parameters agree very well with those experimentally determined using Fourier transform microwave (FTMW)

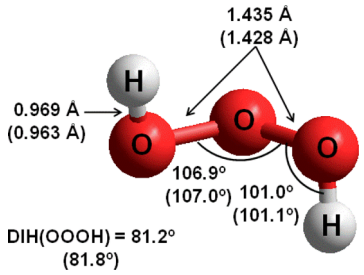

Figure 1. Molecular structure of *trans*-HOOOH derived from CCSD(T)/aug-cc-pVTZ calculations. Experimental values are given in brackets.[33]

spectroscopy and FTMW-millimeter-wave double resonance and triple resonance spectroscopy techniques.[33] In fact, a comparison between calculated and experimental bond lengths and bond angles leads to mean absolute deviations (MAD) of 0.007 Å and 0.3°, respectively. The short O−O bond lengths, 1.435 Å, are similar to those recently predicted for some fluorinated trioxides[39] and suggest a relatively large stability. Another important structural characteristic of trioxides is the ROOO dihedral angle. In the case of HOOOH (C_2 symmetry), both dihedral angles are equal to 81.2°. The found values for the O−O bond lengths and dihedral angles have been mainly attributed to dipole and the hyperconjugation effects.[40,41]

The HOOOH harmonic vibrational frequencies (unscaled) computed at the CCSD(T)/aug-cc-pVTZ level are listed in Table 1. In addition, approximate mode assignments obtained from the animation of the normal modes are included in this table. The calculated frequencies for HOOOH are in very good agreement with those obtained in an argon matrix.[32] In fact, a relatively small MAD value of 69 cm^{-1} was derived from these data.

Table 1. Harmonic Vibrational Frequencies (in cm^{-1}) and Approximate Assignments of HOOOH Calculated at the CCSD(T)/aug-cc-pVTZ Level

approximated assignments	experimental[a]	calculated
asymmetric HO stretching	3529.6	3731
symmetric HO stretching	3529.6	3728
HOO bending	1359.1	1391
HOO bending	1347.4	1382
symmetric OO stretching	821.0	896
asymmetric OO stretching	776.3	798
OOO bending	509.1	521
HOO torsion	387.0	417
HOO torsion	346.4	361

[a]Reference 32.

3.2. Energetics and Potential Energy Curves for HO + HO_2 → HOOOH. As above-mentioned, several experimental and theoretical studies have dealt with the kinetics of the reaction between HO and HO_2 radicals.[1,11,13,14,42] The slight pressure dependence observed for this process has been explained via the formation of the HOOOH. However, the transition state leading to the formation of H_2O + $^1O_2$ in reaction 1a is located 44.1 kcal mol^{-1} above of HOOOH (or 13.6 kcal mol^{-1} above of the HO + HO_2 radicals) at the CCSD(T)/aug-cc-pVTZ//CCSD/aug-cc-pVDZ level of theory for a singlet potential energy surface. Therefore, except at very high temperatures and in concordance with the investigations

DOI: 10.1021/acs.jpca.6b10427
J. Phys. Chem. A 2017, 121, 440−447

of Kaiser and co-workers,[14,42] the HO and HO_2 radicals recombine forming HOOOH. The above discussion is schematized in Figure 2. It is important to note that the

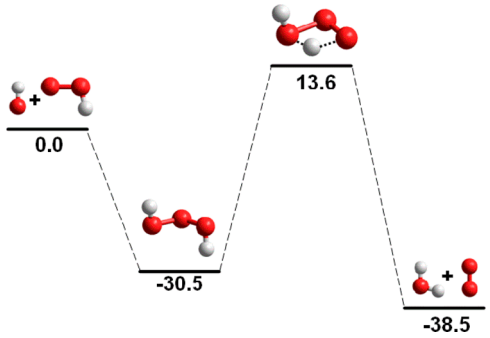

Figure 2. Schematic diagram (in kcal mol^{-1}) for a singlet potential energy surface of the HO + HO_2 reaction calculated at the CCSD(T)/aug-cc-pVTZ//CCSD/aug-cc-pVDZ level of theory.

experimental value for the enthalpy of the reaction HO + HO_2 → H_2O + $^1O_2$ is −47.1 kcal mol^{-1} at 0 K, underestimated at the CCSD(T)/aug-cc-pVTZ//CCSD/aug-cc-pVDZ level, mainly due to errors in the calculations of the excited species $^1O_2$. This result is improved to −42.3 kcal mol^{-1} at the G4 level. However, the analysis of this last reaction is beyond the scope of our work.

According to CCSD(T)/aug-cc-pVTZ//CCSD(T)/aug-cc-pVDZ calculations, a bond dissociation energy of $D_e = \Delta_0 H^0 + \Delta E_{ZPE}$ = 35.5 kcal mol^{-1} is predicted for the HOOOH → HO + HO_2 reaction. The calculated $\Delta_0 H^0$ values of 30.5 kcal mol^{-1} (CCSD(T)/aug-cc-pVTZ//CCSD(T)/aug-cc-pVDZ) and 30.7 kcal mol^{-1} (CCSD(T)/aug-cc-pVTZ) agree satisfactorily with the derived from recommended enthalpies of formation at 0 K, 31.89 kcal mol^{-1},[2] and with the MP4/6-31G(d,p) value of 29.09 kcal mol^{-1},[14] but differ significantly from the value of 21.9 kcal mol^{-1} computed at the CI/ANO level.[14,43]

Potential energy curves for HO + HO_2 → HOOOH along the minimum energy path (MEP) were obtained at different levels of theory. For each O−O bond distance a full optimization of the other HOOOH geometrical parameters was allowed. The resulting normalized curves, V/D_e, at the G3(MP2)//B3LYP/6-311++G(3df,3pd), G4(MP2)//B3LYP/6-311++G(3df,3pd), G4, and CCSD(T)/aug-cc-pVTZ//CCSD(T)/aug-cc-pVDZ levels are depicted in Figure 3. The employed D_e values have been derived from the total energies of the HO, HO_2 and HOOOH species. To our knowledge, these are the first potential energy calculations for HOOOH. As can be seen, all selected methods predict long-range and smooth potential curves, but not so large as those resulting from dipole−dipole interactions (see below).[13,14,44] As Table 2 shows, the derived normalized potentials can be well fitted with a Morse function, $V/D_e = [1 - \exp(-\beta(r - r_e)]^2$, with β parameters ranging between 2.75 and 3.05 $Å^{-1}$.

To perform the kinetic study of k_∞, besides the above isotropic potential, the anisotropic part of the potential surface arising from the contribution of the degrees of freedom orthogonal to the reaction coordinate must be characterized. These transitional modes change from pure vibrational modes, at the HOOOH equilibrium bond distance, to totally free rotations of the HO and HO_2 radicals at large O−O interfragment distances. Quantum-chemical calculations show that only the four lowest vibrational frequencies exhibit a

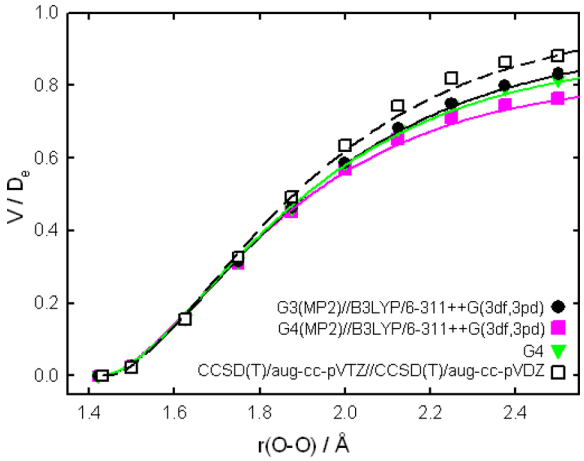

Figure 3. Normalized radial potential curves calculated along the MEP for HO + HO_2 → HOOOH. For the fits, see the text.

Table 2. Bond Dissociation Energies (in kcal mol^{-1}) and Morse Parameters β (in $Å^{-1}$) Derived from the Fits of Figure 3

level of theory	D_e	β
G3(MP2)//B3LYP/6-311++G(3df,3pd)	35.1	2.75
G4(MP2)//B3LYP/6-311++G(3df,3pd)	35.4	3.05
G4	36.0	2.79
CCSD(T)/aug-cc-pVTZ//CCSD(T)/aug-cc-pVDZ	35.5	2.80

pronounced decay as the HO−OOH bond distances increase. The values of the transitional frequencies for reaction 1b along the MEP are listed in Table 3. They can be well described by the expression $\nu_r \approx \nu_e \exp[-\alpha(r - r_e)]$, where α is the so-called anisotropy parameter.[45] The respective CCSD(T)/aug-cc-pVDZ values are α_1 = 1.45, α_2 = 1.24, α_3 = 1.13, and α_4 = 0.858 $Å^{-1}$. The resulting average value of 1.17 ± 0.25 $Å^{-1}$ is similar to the derived from the analysis of a large number of experimental recombination reactions, 1.09 ± 0.30 $Å^{-1}$,[29] with a simplified SACM model.[28] For a comparison, similar calculations performed at the B3LYP/6-311++G(3df,3pd) and B2PLYP/6-311++G(3df,3pd) levels (see Table 3) lead to α values of 1.45, 1.16, 0.83, and 0.332 $Å^{-1}$ and 1.56, 1.04, 0.97, and 0.451 $Å^{-1}$, respectively. The resulting average values of 0.943 and 1.01 $Å^{-1}$ are also reasonable for this type of recombination reactions.

3.3. High Pressure Rate Coefficients for HO + HO_2 → HOOOH. The high pressure rate coefficients for the recombination reaction HO + HO_2 → HOOOH were calculated using the SACM/CT approach,[25−27] employing the potential energy surface properties described in sections 3.1 and 3.2. The HO_2 radical was treated as a quasi-linear species, forming with the HO a nonlinear adduct with an angle θ between the rotor axis and the molecular axis connecting the center of mass of the fragments.

The procedure to estimate SACM/CT high pressure rate coefficients has been described previously.[46,47] It has been demonstrated that the high pressure rate coefficients can be factorized as[29]

$$k_\infty = f_{rigid} k^{PST}{}_\infty \quad (2)$$

Here $k_\infty{}^{PST}$ is the phase space theory rate coefficient which is computed with the isotropic part of the potential, and f_{rigid} is a

DOI: 10.1021/acs.jpca.6b10427
J. Phys. Chem. A 2017, 121, 440−447

Table 3. Calculated Transitional Frequencies (in cm^{-1}) for Reaction HO + HO_2 → HOOOH as a Function of the O−O Bond Length (in Å)[a]

	ν_1(torsion)			ν_2(torsion)			ν_3(OOO bending)			ν_4(OOO asymmetric stretching)		
r(O−O)	a	b	c	a	b	c	a	b	c	a	b	c
r_e	364	375	372	423	431	431	507	535	536	734	804	806
1.500	347	340	337	424	446	442	491	512	510	652	674	663
1.625	284	280	272	337	381	347	456	490	478	515	556	548
1.750	–	–	–	256	267	259	412	447	436	526	574	573
1.875	–	–	–	226	226	230	359	400	386	534	588	590
2.000	–	–	–	200	202	210	306	355	338	516	584	582
2.125	–	–	–	182	181	194	257	315	294	479	567	555
2.250	–	–	–	167	160	180	212	279	255	417	541	514
2.375	–	–	–	143	150	163	175	249	221	331	510	462
2.500	–	–	–	106	138	146	170	222	191	216	478	402

[a]Key: a, CCSD(T)/aug-cc-pVDZ (r_e = 1.451 Å); b, B3LYP/6-311++G(3df,3pd) (r_e = 1.422 Å); c, B2PLYP/6-311++G(3df,3pd) (r_e = 1.423 Å).

rigidity factor that accounts for dynamical constraints due to the anisotropy of the electronic potential.

k_∞^{PST} can be calculated as

$$k_\infty^{PST} = f_e f_{sym} (8\pi kT/\mu)^{1/2} (31.153 - 18.158X + 0.8685X^2)/\beta^2 \quad (3)$$

where $X = \ln(kT/D_e) - \beta r_{CM} + 4$.[26] For the present reaction, the collisional reduced mass μ = 11.22 g mol^{-1}, the electronic degeneracy factor at 298 K $f_e = Q_{elHOOOH}/Q_{elHO}Q_{elHO2}$ = 0.166 (where a spin−orbit splitting of 139.7 cm^{-1} was considered for OH[12]), the stoichiometric coefficient f_{sym} = 1 and the distance between the centers of mass of the two combining radicals r_{CM} = 1.87 Å were calculated.

An earlier expression to estimate k_∞^{PST} is given by

$$k_\infty^{PST} = f_e (kT/h)(h^2/2\pi\mu kT)^{3/2} Q_{cent} \quad (4)$$

where Q_{cent} is the centrifugal pseudopartition function.[28]

On the other hand, f_{rigid} is given by[26]

$$f_{rigid} \approx [1 - 2.3C_{eff}(\beta r_{CM})^{1/2} \exp((X-4)/2.044)] (1 + 0.75Z + Z^4)^{-1/4} \quad (5)$$

with[27]

$$Z = (dC_{eff})^n \quad (6)$$

$$C_{eff} = \{1 + 0.4[2\alpha/\beta - 1] + [2\alpha/\beta - 1]^2\} \{[2\varepsilon_s^2\varepsilon_a^2\varepsilon_t^2/[B_1B_2(B_1+B_2)]]^{1/3}\} /2D_e\{kT/D_e\}^{2\alpha/\beta-1} \quad (7)$$

$$n = 1 - 0.5\sin^2\theta + \sin^4\theta \quad (8)$$

$$d = 1.757 - 1.337\sin^2\theta - 0.393/\sin^2\theta + [(\varepsilon_a/\varepsilon_t)(\varepsilon_s/\varepsilon_t)]^{2/3}(1.444 - 0.509\sin^2\theta - 0.07730/\sin^2\theta) + (\varepsilon_a/\varepsilon_t)^2 \cos^2\theta(0.357 - 0.557\sin^2\theta + 0.247/\sin^2\theta) + (\varepsilon_s/\varepsilon_t)^2\cos^2\theta(-1.932 + 0.385\sin^2\theta + 1.529/\sin^2\theta) \quad (9)$$

In the above equations, θ = 87.1°; ε_s = 521, ε_a = 798, and ε_t = 361 cm^{-1} are the adduct vibrational frequencies for the symmetrical and asymmetrical deformation modes and for the torsional motion, B_1 = 18.772 cm^{-1} is the HO rotational constant, and B_2 = 1.084 cm^{-1} is the average of the smallest HO_2 rotational constants, all calculated at the CCSD(T)/aug-cc-pVTZ level of theory.

Additionally, using the simplified SACM version of refs 28 and 29, f_{rigid} can be calculated by

$$f_{rigid} = (F_{AM}/\sigma)\frac{\prod_{m=1}^{5} Q_m \prod_{j=1}^{4} Q_j}{Q_{rotHO}Q_{rotHO2}Q_{vibHO}Q_{vibHO2}} e^{-\Delta E_{0z}/kT} \approx (F_{AM}/\sigma)\frac{\prod_{m=1}^{5} Q_m}{Q_{rotHO}Q_{rotHO2}} e^{-\Delta E_{0z}/kT} \quad (10)$$

Here, F_{AM} is an angular momentum coupling correction factor, σ is an effective symmetry number, Q_m and Q_j are the pseudopartition functions corresponding to the transitional modes and the conserved oscillators, respectively, Q_{rot} and Q_{vib} are the rotational and vibrational partition functions of HO and HO_2 radicals and, ΔE_{0z} is the adiabatic zero point barrier for the lowest reaction channel. The calculation of the above-mentioned factors was performed from the molecular data listed in Tables 1 and 4. The scheme that correlates the highest rotational constant of HOOOH with the lowest rotational constant of HO_2, and the vibrational frequencies corresponding to the transitional modes with the rest of the rotational constants of HO and HO_2 radicals is the following (in cm^{-1}): 1.694 ↔ 1.055 (m = 1), 361 ↔ 1.112 (m = 2), 416 ↔ 18.773 (m = 3), 521 ↔ 18.773 (m = 4), 798 ↔ 20.505 (m = 5). The effective rotational constant was calculated with the expression $B_{eff}(r) = [B(r) + C(r)]/2 = 0.3299/[1 + 0.430(r - r_e) + 0.484(r - r_e)^2]$, with r_e = 1.451 Å, resulting from the CCSD(T)/aug-cc-pVDZ geometries along the MEP.

Table 4. Calculated Harmonic Vibrational Frequencies and Rotational Constants (both in cm^{-1}) for HOOOH, HO and HO_2 at the CCSD(T)/aug-cc-pVTZ Level

species	frequencies	rotational constants
HOOOH	3731, 3728, 1391, 1382, 896, 798, 521, 417, 361	0.313, 0.357, 1.694
HO	3719	18.773
HO_2	3646, 1428, 1125	1.055, 1.112, 20.505

DOI: 10.1021/acs.jpca.6b10427
J. Phys. Chem. A 2017, 121, 440−447

Table 5. Calculated High Pressure Rate Coefficients k_∞^{PST} and k_∞ (in cm^3 molecule^{-1} s^{-1}) and Rigidity Factors for HO + HO$_2$ → HOOOH. (T in K)

T	k_∞^{PST}[eq 3]	k_∞^{PST}[eq 4]	f_{rigid}[eq 5]	f_{rigid}[eq 10]	k_∞(SACM/CT)	k_∞(simplified SACM)
200	7.40×10^{-11}	8.56×10^{-11}	0.0446	0.0321	3.30×10^{-12}	2.75×10^{-12}
250	7.51×10^{-11}	8.60×10^{-11}	0.0456	0.0343	3.42×10^{-12}	2.95×10^{-12}
298	7.62×10^{-11}	8.67×10^{-11}	0.0463	0.0356	3.53×10^{-12}	3.09×10^{-12}
350	7.75×10^{-11}	8.75×10^{-11}	0.0470	0.0366	3.64×10^{-12}	3.20×10^{-12}
400	7.87×10^{-11}	8.84×10^{-11}	0.0475	0.0371	3.74×10^{-12}	3.28×10^{-12}
450	7.99×10^{-11}	8.94×10^{-11}	0.0480	0.0373	3.84×10^{-12}	3.33×10^{-12}
500	8.11×10^{-11}	9.04×10^{-11}	0.0483	0.0372	3.92×10^{-12}	3.36×10^{-12}
550	8.23×10^{-11}	9.13×10^{-11}	0.0487	0.0369	4.01×10^{-12}	3.37×10^{-12}
600	8.34×10^{-11}	9.23×10^{-11}	0.0489	0.0351	4.08×10^{-12}	3.37×10^{-12}

For both kinetics models, the CCSD(T)/aug-cc-pVTZ//CCSD(T)/aug-cc-pVDZ curve fitted with the parameters β = 2.80 Å^{-1} and D_e = 35.5 kcal mol^{-1} was employed. The looseness parameter α = 1.17 Å^{-1} derived at the CCSD(T)/aug-cc-pVDZ level, was used in the f_{rigid} calculations.

With the more recent SACM approach given by eqs 3 and 5, values of k_∞^{PST} = 7.62×10^{-11} cm^3 molecule^{-1} s^{-1} and f_{rigid} = 0.046 were obtained at 298 K. As a consequence, according to expression 2, the SACM/CT value of 3.53×10^{-12} cm^3 molecule^{-1} s^{-1} was derived for k_∞. This value becomes about 2.7 times smaller for α = 0.943 Å^{-1} (B3LYP/6-311++G(3df,3pd)), and decreases by about a factor of 2 if α = 1.01 Å^{-1} (B2PLYP/6-311++G(3df,3pd)) is used. On the other hand, from the expressions 4 and 10, k_∞^{PST} = 8.68×10^{-11} cm^3 molecule^{-1} s^{-1} and f_{rigid} = 0.036 were derived, leading to the SACM value k_∞ = 3.09×10^{-12} cm^3 molecule^{-1} s^{-1} at 298 K. Therefore, the simplified SACM and the SACM/CT results differ by only 12%.

The high pressure rate coefficients calculated between 200 and 600 K using the simplified SACM and the SACM/CT approaches are summarized in Table 5 and can be expressed by

$$k_\infty = 3.55 \times 10^{-12}(T/300)^{0.20} \text{ cm}^3 \text{ molecule}^{-1} \text{ s}^{-1} \quad \text{(SACM/CT)} \tag{11}$$

$$k_\infty = 3.05 \times 10^{-12}(T/300)^{0.18} \text{ cm}^3 \text{ molecule}^{-1} \text{ s}^{-1} \quad \text{(simplified SACM)} \tag{12}$$

That is, both SACM theories lead to comparable results. By contrast, the room temperature SACM/CT rate coefficient is 13−29 times smaller than theoretical values reported 25 years ago. In fact, values of 4.72×10^{-11} cm^3 molecule^{-1} s^{-1} (vibrational/rotational adiabatic capture rate theory),[14] 9.75×10^{-11} cm^3 molecule^{-1} s^{-1} (modified Langevin collision capture model)[48] and 1.02×10^{-10} cm^3 molecule^{-1} s^{-1} (canonical variational transition state theory, CVTST)[14] have been predicted for k_∞. For all these cases the long-range of the potential was approached by a dipole−dipole interaction potential,

$$V = -(\mu_1\mu_2/r^3)[2 \cos\theta_1 \cos\theta_2 - \sin\theta_1 \sin\theta_2 \cos(\phi_1 - \phi_2)] \tag{13}$$

Here μ_i are the dipole moments of the reactants (1.67 D for HO[49] and 2.09 D for HO$_2$[50]), while θ_i and ϕ_i are the spherical polar angles describing the orientation of r_i with respect to the body-fixed axes, for radical i.[14] Figure 4 shows the high energy region of the Morse potential based on the CCSD(T)/aug-cc-pVTZ//CCSD(T)/aug-cc-pVDZ calculations and the dipole−dipole potential for angular contribution values of 1.0 and 0.81. The last one has been derived from the present calculations along the MEP.

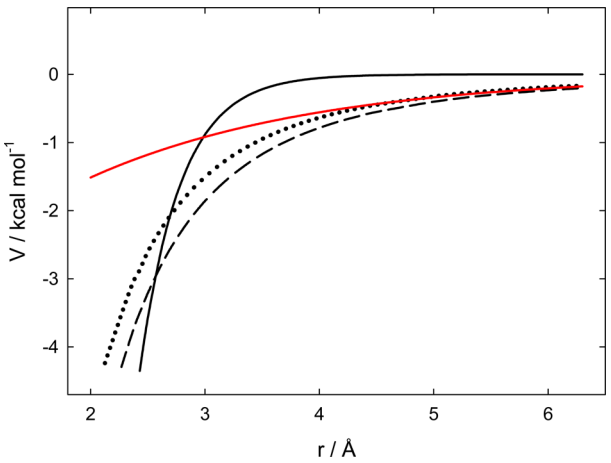

Figure 4. Morse and dipole−dipole potentials for HO + HO$_2$ → HOOOH. Black solid line: Calculated with a Morse parameter of β = 2.80 Å^{-1}. Black dotted line: Calculated with an angular contribution of 1.0 in eq 13. Black dashed line: Calculated with an angular contribution of 0.81 as obtained from CCSD(T)/aug-cc-pVDZ calculations along the MEP. Red solid line: Fit of the dipole−dipole potential at large elongations with a Morse function with $\beta_{d\text{-}d}$ = 0.5 Å^{-1}.

It can be seen that the dipole−dipole potential leads to a pronounced attractive interaction between the reagents. To compare the rate data predicted by both potentials, k_∞^{PST} calculations were performed at 298 K. For this, the higher part of the dipole−dipole potential was fitted with a Morse function using the very low value $\beta_{d\text{-}d}$ = 0.5 Å^{-1} (see Figure 4). The simple eq 3 predicts a value of 7.9×10^{-10} cm^3 molecule^{-1} s^{-1} when this parameter is employed. This k_∞^{PST} is 1 order of magnitude larger (see Table 5) than the value derived using the ab initio potential. However, despite the inherent differences between the vibrational/rotational adiabatic capture rate theory and the SACM/CT, similar $f_{rigid} = k_\infty/k_\infty^{PST}$ values of 0.06 and 0.05 were respectively obtained. However, a f_{rigid} nearly a factor of 2 larger results from modified Langevin collision capture and CVTST calculations.[14] These results indicate that the pronounced rate coefficient discrepancies between earlier and the present calculations are mostly attributed to the unrealistically large dipole−dipole potential employed in ref 14.

3.4. Low Pressure Rate Coefficients for HO + HO$_2$ + He → HOOOH + He. To investigate the pressure dependence of present reaction, the limiting low pressure rate coefficients, k_0, and the relevant falloff curves are required. k_0 was calculated

DOI: 10.1021/acs.jpca.6b10427
J. Phys. Chem. A 2017, 121, 440−447

Table 6. Contributing Factors to k_0 for Reaction HO + HO_2 + He → HOOOH + He (Z_{LJ} and k_0 in cm^3 molecule $^{-1}$ s^{-1}, K_C in molecules cm^{-3}, and T in K)

T	Z_{LJ}	F_E	F_{rot}	F_{rotint}	Q_{vib}	β_c	K_C	k_0/[He]
200	3.41×10^{-10}	1.07	20.08	32.81	1.03	0.251	1.23×10^{-8}	5.95×10^{-31}
250	3.63×10^{-10}	1.09	15.74	25.41	1.07	0.213	9.33×10^{-2}	2.75×10^{-31}
298	3.82×10^{-10}	1.11	12.94	20.49	1.13	0.186	2.56×10^{3}	1.54×10^{-31}
350	4.01×10^{-10}	1.13	10.81	16.70	1.22	0.163	6.46×10^{6}	9.22×10^{-32}
400	4.17×10^{-10}	1.16	9.28	14.00	1.32	0.145	1.76×10^{9}	6.07×10^{-32}
450	4.32×10^{-10}	1.18	8.11	11.94	1.45	0.131	1.35×10^{11}	4.25×10^{-32}
500	4.47×10^{-10}	1.20	7.18	10.33	1.61	0.118	4.24×10^{12}	3.06×10^{-32}
550	4.60×10^{-10}	1.23	6.42	9.04	1.79	0.108	6.99×10^{13}	2.30×10^{-32}
600	4.73×10^{-10}	1.25	5.80	8.00	2.00	0.099	7.11×10^{14}	1.76×10^{-32}

using Troe's factorized formalism.[23,24] In this approach, the recombination low pressure rate coefficient is represented by the product $k_0 = \beta_c k_0^{SC}$, where the collision efficiency β_c depends on intermolecular energy transfer properties and the strong-collision rate coefficient k_0^{SC} is characterized by the equilibrium populations of molecular states. The different terms contributing to k_0^{SC} are explicitly accounted for by[23]

$$k_0^{SC} = (1/K_C)[M]Z_{LJ}(\rho_{vib,h}(E_0)kT/Q_{vib}) \exp(-E_0/kT)F_{anh}F_E F_{rot}F_{rotint} \quad (14)$$

Here, $K_C = [HO][HO_2]/[HOOOH]$ is the equilibrium constant estimated from the molecular partition functions and the threshold energy $E_0 \approx \Delta_0 H^0 = 30.7$ kcal mol^{-1}, Z_{LJ} is the collision frequency between the energized HOOOH adduct and the bath gas M = He, $\rho_{vib,h}(E_0)$ is the HOOOH harmonic vibrational density of states at E_0, Q_{vib} is the HOOOH vibrational partition function, and the F factors are corrections for different effects. F_{anh} takes into consideration the anharmonicity, F_E accounts for the energy dependence of $\rho_{vib,h}(E_0)$, F_{rot} describes the external rotations contribution, and finally F_{rotint} takes into account the internal rotors behavior. The evaluation of these factors was performed using the molecular data listed in Tables 1 and 4. In particular, the 8.84×10^2 (kcal $mol^{-1})^{-1}$ and 1.38 values were estimated for $\rho_{vib,h}(E_0)$ and F_{anh}, respectively. The potential energy curve computed at the CCSD(T)/aug-cc-pVTZ//CCSD(T)/aug-cc-pVDZ level was employed for the F_{rot} calculations (Figure 3). Barrier heights of 4.5 kcal mol^{-1} and reduced moments of inertia of 0.87 amu $Å^2$ were obtained for the HOO−OH internal rotations from CCSD(T)/aug-cc-pVTZ//CCSD/aug-cc-pVDZ calculations. Lennard-Jones collision parameters for HOOOH of, σ = 3.8 Å and ε/k = 289.3 K, employed in the calculation of Z_{LJ} were derived considering additivity relationships for molar volumes and by molecular resemblance to HOOH,[12,51] while values of 2.55 Å and ε/k = 10 K were used for He.[52]

Table 6 summarizes estimated factors in eq 14 and the resulting K_C and k_0 values obtained between 200 and 600 K. The β_c values were derived from the expression $-\langle\Delta E\rangle \approx F_E kT\beta_c/(1 - \beta_c^{1/2})$,[23] assuming that the average energy transferred in up and down HOOOH−He collisions, $-\langle\Delta E\rangle \approx 75$ cm^{-1}, does not change between 200 and 600 K.[52]

The results obtained can be represented by

$$k_0 = [He]1.55 \times 10^{-31}(T/300)^{-3.2} \text{ cm}^3 \text{ molecule}^{-1} \text{ s}^{-1} \quad (15)$$

3.5. Rate Coefficients for HO + HO_2 + He → HOOOH + He in the Falloff Range. The kinetic behavior of the HO + HO_2 + He → HOOOH + He reaction in the intermediate region between the low and the high pressure limits, the falloff range, was theoretically investigated. To this end, we employed the Troe's reduced method,[30,31] in which the rate coefficients are estimated using the following relationship

$$k \approx k_\infty[x/(1 + x)]F(x) \quad (16)$$

where $F(x)$ are suitable broadening factors and $x = k_0/k_\infty$. These factors account for corrections to the Lindemann−Hinshelwood expression (indicated between brackets in eq 16) due to the energy and total angular momentum dependencies of the energized adducts and the multistep character of the collisional energy transfer. These broadening factors are given by[31]

$$F(x) = [1 + x]/[1 + x^n]^{1/n} \quad (17)$$

Here $n = [\ln 2/\ln(2/F_{cent})][0.8 + 0.2x^q]$, $q = (F_{cent} - 1)/\ln(F_{cent}/10)$, and the center broadening factor is given by $F_{cent} = F(x = 1)$. For low temperatures applications, a constant value of F_{cent} = 0.6 is usually employed.[2] However, for a more reliable analysis, F_{cent} can be estimated from the weak, log $F_{cent}^{WC} = 0.14 \log \beta_c$, and strong collision, F_{cent}^{SC}, contributions: $F_{cent} = F_{cent}^{WC}F_{cent}^{SC}$. The strong collision broadening factor is given by $-\log F_{cent}^{SC} = (1.06 \log S_T)^{2.2}/(1 + C_1 S_T^{C_2})$, with $C_1 = 0.10 \exp(2.5 B_T^{-1} - 0.22B_T - 6 \times 10^{-10}B_T^6)$ and $C_2 = 1.9 + 4.6 \times 10^{-5}B_T^{2.8}$.[30] The Kassel parameters S_T and B_T were calculated employing the harmonic vibrational frequencies listed in Table 1 and $\Delta_0 H^0$ = 30.7 kcal mol^{-1}. To estimate the F_{cent}^{WC} factors, β_c values from Table 6 were employed. The F_{cent} values obtained decrease from 0.67 to 0.42 when the temperature increases from 200 to 600 K.

The resulting falloff curves are shown in Figure 5. The two straight lines, drawn for simplicity only for 300 K, allow to visualize the center of the falloff curves, $[He]_c = k_\infty/k_0[He]$. It is observed that at room temperature and atmospheric pressure ($\sim 2.5 \times 10^{19}$ molecules cm^{-3} or ~1.013 bar) the reaction is close to the high pressure limit. In addition, for a given total pressure, the predicted k decreases as the temperature increases. For comparison, RRKM falloff curves derived by Gonzalez et al. at 300 K are included in Figure 5.[14] As can be seen, these estimations obtained from molecular information provided by MP4/6-31G(d,p) and CI/ANO energetics, give different pressure dependencies. At about 1 atm of He, the CI/ANO based and our falloff curve are close. Below $\sim 10^{17}$ molecules cm^{-3}, the present results lie between those obtained in ref 14. based on MP4/6-31G(d,p) and CI/ANO quantum-chemical data. Above 1 atm, the long-range dipole−dipole potential employed in the k_∞ estimations of ref 14 is the principal reason for the observed differences.

DOI: 10.1021/acs.jpca.6b10427
J. Phys. Chem. A 2017, 121, 440−447

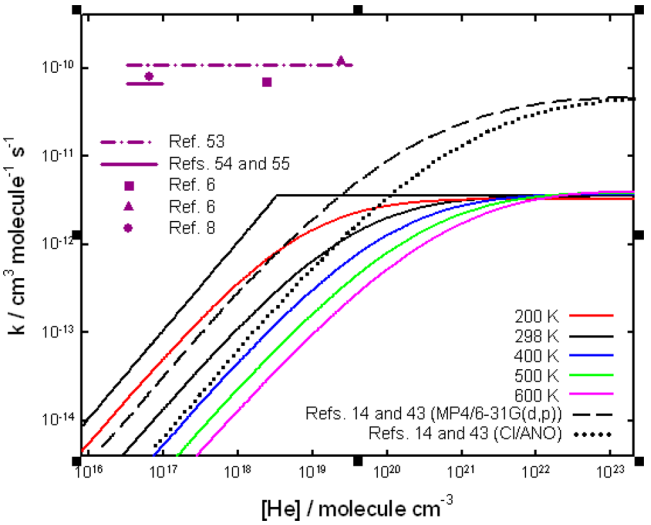

Figure 5. Falloff curves for HO + HO_2 + He → HOOOH + He. Violet: rate coefficient data for HO + HO_2 → H_2O + O_2 at 298 K.

Finally, representative data for the reaction 1a, HO + HO_2 → H_2O + O_2, are also shown in Figure 5. These values are quite consistent with the consensus value of k_{1a} = 4.8 × 10^{-11} exp(250/T) cm^3 $molecule^{-1}$ s^{-1}.[2−4] A comparison of these values with present k_{1b} results clearly indicates that the association process is irrelevant in all experimental conditions. By contrast, it has been suggested that above 5000 Torr (~1.6 × 10^{20} molecules cm^{-3}) reaction 1b could compete with reaction 1a.[14] Therefore, the small pressure dependence observed for the HO + HO_2 global reaction from k ~ (5−8) × 10^{-11} cm^3 $molecule^{-1}$ s^{-1} (at 1−75 Torr of refs 6, 11, 54, and 55) to k ~ (1−2) × 10^{-10} cm^3 $molecule^{-1}$ s^{-1} (at about 1 atm[6,53]), may be probably attributed, as Keyser et al. suggested,[56] to secondary reactions arising from the presence of small concentrations of H and O atoms in the low pressure discharge-flow investigations.

4. CONCLUSIONS

The kinetics of the recombination reaction HO + HO_2 + He → HOOOH + He has been theoretically studied on the singlet potential energy surface. SACM/CT and unimolecular rate theory calculations on CCSD(T)/aug-cc-pVTZ//CCSD(T)/aug-cc-pVDZ electronic potential allow to estimate the rate coefficient over a wide range of pressures and temperatures. The derived high and low pressure rate coefficients between 200 and 600 K are given by k_∞ = 3.55 × 10^{-12} $(T/300)^{0.20}$ cm^3 $molecule^{-1}$ s^{-1} and k_0 = [He] 1.55 × 10^{-31} $(T/300)^{-3.2}$ cm^3 $molecule^{-1}$ s^{-1}. The present rate coefficients are much smaller than those measured for the HO + HO_2 → H_2O + O_2 reaction, indicating that the association pathway studied here does not play any role in any experimental condition.

AUTHOR INFORMATION

Corresponding Author

*(M.P.B.) Telephone: +54-221-4257430. Fax: +54-221-4254642. E-mail: mbadenes@inifta.unlp.edu.ar.

ORCID

María P. Badenes: 0000-0003-1157-4790

Notes

The authors declare no competing financial interest.

ACKNOWLEDGMENTS

This research project was supported by the Universidad Nacional de La Plata (11/X676), the Consejo Nacional de Investigaciones Científicas y Técnicas CONICET (PIP-0134, PIP-1134), and the Agencia Nacional de Promoción Científica y Tecnológica (PICT-478, PICT-2425).

REFERENCES

(1) Sridharan, U. C.; Qiu, L. X.; Kaufman, F. Rate Constant of the OH + HO_2 Reaction from 252 to 420 K. *J. Phys. Chem.* **1984**, *88*, 1281−1282.

(2) Sander, S. P.; Friedl, R. R.; Barker, J. R.; Golden, D. M.; Kurylo, M. J.; Wine, P. H.; Abbatt, J. P. D.; Burkholder, J. B.; Kolb, C. E.; Moortgat, G. K.; Huie, R. E.; Orkin, V. L. *Chemical Kinetics and Photochemical Data for Use in Atmospheric Studies*; NASA/JPL Data Evaluation, JPL Publication 06-2 Evaluation No. 17, NASA: Pasadena, CA, June 1, 2011; http://jpldataeval.jpl.nasa.gov/.

(3) Atkinson, R.; Baulch, D. L.; Cox, R. A.; Crowley, J. N.; Hampson, R. F.; Hynes, R. G.; Jenkin, M. E.; Rossi, M. J.; Troe. *Atmos. Chem. Phys.* **2004**, *4*, 1461−1738. IUPAC Task Group on Atmospheric Chemical Kinetic Data Evaluation, Vol 1, http://iupac.pole-ether.fr.

(4) Baulch, D. L.; Bowman, C. T.; Cobos, C. J.; Cox, R. A.; Just, Th.; Kerr, J. A.; Pilling, M. J.; Stocker, D.; Troe, J.; Tsang, W.; Walker, J.; Warnatz, J. Evaluated Kinetic Data for Combustion Modeling: Supplement II. *J. Phys. Chem. Ref. Data* **2005**, *34*, 757−1397.

(5) Hong, Z.; Vasu, S. S.; Davidson, D. F.; Hanson, R. K. Experimental Study of the Rate of OH + HO_2 → H_2O + O_2 at High Temperatures Using the Reverse Reaction. *J. Phys. Chem. A* **2010**, *114*, 5520−5525.

(6) DeMore, W. B. Rate Constant and Possible Pressure Dependence of the Reaction OH + HO_2. *J. Phys. Chem.* **1982**, *86*, 121−126.

(7) Cerkovnik, J.; Plesničar, B. Recent Advances in the Chemistry of Hydrogen Trioxide (HOOOH). *Chem. Rev.* **2013**, *113*, 7930−7951.

(8) Denis, P. A.; Ornellas, F. R. Theoretical Characterization of Hydrogen Polyoxides: HOOH, HOOOH, HOOOOH, and HOOO. *J. Phys. Chem. A* **2009**, *113*, 499−506.

(9) Lay, T. H.; Bozzelli, J. W. Enthalpies of Formation and Group Additivity of Alkyl Peroxides and Trioxides. *J. Phys. Chem. A* **1997**, *101*, 9505−9510.

(10) Grant, D. J.; Dixon, D. A.; Francisco, J. S.; Feller, D.; Peterson, K. A. Heats of Formation of the $H_{1,2}O_mS_n$ (m, n = 0−3) Molecules from Electronic Structure Calculations. *J. Phys. Chem. A* **2009**, *113*, 11343−11353.

(11) Schwab, J. J.; Brune, W. H.; Anderson, J. G. Kinetics and Mechanism of the OH + HO_2 Reaction. *J. Phys. Chem.* **1989**, *93*, 1030−1035.

(12) *NIST Chemistry WebBook*; NIST Standard Reference Database Number 69, http://webbook.nist.gov/chemistry.

(13) Mozurkewich, M. Reactions of HO_2 with Free Radicals. *J. Phys. Chem.* **1986**, *90*, 2216−2221.

(14) Gonzalez, C.; Theisen, J.; Zhu, L.; Schlegel, H. B.; Hase, W. L.; Kaiser, E. W. Kinetics of the Reaction between OH and HO_2 on the Singlet Potential Energy Surface. *J. Phys. Chem.* **1991**, *95*, 6784−6792.

(15) Raghavachari, K.; Trucks, G. W.; Pople, J. A.; Head-Gordon, M. A Fifth-Order Perturbation Comparison of Electron Correlation Theories. *Chem. Phys. Lett.* **1989**, *157*, 479−483.

(16) Dunning, T. H., Jr. Gaussian Basis Sets for Use in Correlated Molecular Calculations. I. The Atoms Boron Through Neon and Hydrogen. *J. Chem. Phys.* **1989**, *90*, 1007−1023.

(17) Baboul, A. G.; Curtiss, L. A.; Redfern, P. C.; Raghavachari, K. Gaussian-3 theory using density functional geometries and zero-point energies. *J. Chem. Phys.* **1999**, *110*, 7650−7657.

(18) Curtiss, L. A.; Redfern, P. C.; Rassolov, V.; Kedziora, G.; Pople, J. E. Extension of Gaussian-3 theory to molecules containing third-row atoms K, Ca, Ga−Kr. *J. Chem. Phys.* **2001**, *114*, 9287−9295.

(19) Curtiss, L. A.; Redfern, P. C.; Raghavachari, K. Gaussian-4 Theory Using Reduced Order Perturbation Theory. *J. Chem. Phys.* **2007**, *127*, 124105.

DOI: 10.1021/acs.jpca.6b10427
J. Phys. Chem. A 2017, 121, 440−447

(20) Curtiss, L. A.; Redfern, P. C.; Raghavachari, K. Gaussian-4 Theory. *J. Chem. Phys.* **2007**, *126*, 084108.
(21) Grimme, S. Semiempirical Hybrid Density Functional with Perturbative Second-Order Correlation. *J. Chem. Phys.* **2006**, *124*, 034108.
(22) Frisch, M. J.; Trucks, G. W.; Schlegel, H. B.; Scuseria, G. E.; Robb, M. A.; Cheeseman, J. R.; Scalmani, G.; Barone, V.; Mennucci, B.; Petersson, G. A. et al. *Gaussian 09*, revision A.02; Gaussian, Inc: Wallingford, CT, 2009.
(23) Troe, J. Theory of Thermal Unimolecular Reactions at Low Pressures. II. Strong Collision Rate Constants. Applications. *J. Chem. Phys.* **1977**, *66*, 4758−4775.
(24) Troe, J. Predictive Possibilities of Unimolecular Rate Theory. *J. Phys. Chem.* **1979**, *83*, 114−126.
(25) Maergoiz, A. I.; Nikitin, E. E.; Troe, J.; Ushakov, V. G. Classical Trajectory and Statistical Adiabatic Channel Study of the Dynamics of Capture and Unimolecular Bond Fission. IV. Valence Interactions Between Atoms and Linear Rotors. *J. Chem. Phys.* **1998**, *108*, 5265−5280.
(26) Maergoiz, A. I.; Nikitin, E. E.; Troe, J.; Ushakov, V. G. Classical Trajectory and Statistical Adiabatic Channel Study of the Dynamics of Capture and Unimolecular Bond Fission. V. Valence Interactions Between Two Linear Rotors. *J. Chem. Phys.* **1998**, *108*, 9987−9998.
(27) Maergoiz, A. I.; Nikitin, E. E.; Troe, J.; Ushakov, V. G. Classical Trajectory and Statistical Adiabatic Channel Study of the Dynamics of Capture and Unimolecular Bond Fission. VI. Properties of Transitional Modes and Specific Rate Constants k(E,J). *J. Chem. Phys.* **2002**, *117*, 4201−4213.
(28) Troe, J. Theory of Thermal Unimolecular Reactions at High Pressures. *J. Chem. Phys.* **1981**, *75*, 226−237.
(29) Cobos, C. J.; Troe, J. Theory of Thermal Unimolecular Reactions at High Pressures. II. Analysis of Experimental Results. *J. Chem. Phys.* **1985**, *83*, 1010−1015.
(30) Troe, J. Theory of Thermal Unimolecular Reactions in the Fall-Off Range. I. Strong Collision Rate Constants. *Ber. Bunsenges. Phys. Chem.* **1983**, *87*, 161−169.
(31) Troe, J.; Ushakov, V. G. Representation of "Broad" Falloff Curves for Dissociation and Recombination Reactions. *Z. Phys. Chem.* **2014**, *228*, 1−10.
(32) Engdahl, A.; Nelander, B. The Vibrational Spectrum of H_2O_3. *Science* **2002**, *295*, 482−483.
(33) Suma, K.; Sumiyoshi, Y.; Endo, Y. The Rotational Spectrum and Structure of HOOOH. *J. Am. Chem. Soc.* **2005**, *127*, 14998−14999.
(34) Plesničar, B.; Kaiser, A.; Ažman, A. Hydrogen Polyoxides. Ab Initio Molecular Orbital Study. *J. Am. Chem. Soc.* **1973**, *95*, 5476−5477.
(35) Blint, R. J.; Newton, M. D. Ab Initio Studies of Interoxygen Bonding in O_2, HO_2, H_2O_2, O_3, HO_3, and H_2O_3. *J. Chem. Phys.* **1973**, *59*, 6220−6228.
(36) Mckay, D. J.; Wright, J. S. How Long Can You Make an Oxygen Chain? *J. Am. Chem. Soc.* **1998**, *120*, 1003−1013.
(37) Martins-Costa, M.; Anglada, J. M.; Ruiz-López, M. F. Structure, Stability, and Dynamics of Hydrogen Polyoxides. *Int. J. Quantum Chem.* **2011**, *111*, 1543−1554.
(38) Hollman, D. S.; Schaefer, H. F., III In Search of the Next Holy Grail of Polyoxide Chemistry: Explicitly Correlated Ab Initio Full Quartic Force Fields for HOOH, HOOOH, HOOOOH, and their Isotopologues. *J. Chem. Phys.* **2012**, *136*, 084302.
(39) Badenes, M. P.; Tucceri, M. E.; Cobos, C. J. Theoretical Study of the Molecular Conformations, Vibrational Frequencies and Thermochemistry of the FC(O)OOO(O)CF, FS(O_2)OOO(O_2)SF and FC(O)OOO(O_2)SF Trioxides. *Comput. Theor. Chem.* **2013**, *1009*, 86−93.
(40) Plesničar, B. Progress in the Chemistry of Dihydrogen Trioxide (HOOOH). *Acta Chim. Slov.* **2005**, *52*, 1−12.
(41) Martins-Costa, M.; Anglada, J. M.; Ruiz-López, M. F. Hyperconjugation in Adjacent OO Bonds: Remarkable Odd/Even Effects. *Chem. Phys. Lett.* **2009**, *481*, 180−182.
(42) Gonzalez, C.; Theisen, J.; Schlegel, H. B.; Hase, W. L.; Kaiser, E. W. Kinetics of the Reaction between OH and HO, on the Triplet Potential Energy Surface. *J. Phys. Chem.* **1992**, *96*, 1767−1774.
(43) Jackels, C. F.; Phillips, D. H. An Ab Initio Investigation of Possible Intermediates in the Reaction of the Hydroxyl and Hydroperoxyl Radicals. *J. Chem. Phys.* **1986**, *84*, 5013−5024.
(44) Phillips, L. F. Calculation of Langevin-Type Capture Rate Constants for Rotating Molecules with Arbitrary Interaction Potentials. *J. Comput. Chem.* **1990**, *11*, 88−93.
(45) Quack, M.; Troe, J. Specific Rate Constants of Unimolecular Processes II. Adiabatic Channel Model. *Ber. Bunsenges. Phys. Chem.* **1974**, *78*, 240−252.
(46) Badenes, M. P.; Tucceri, M. E.; Cobos, C. J. Formation and Dissociation Kinetics of the FC(O)OOO(O)CF, FS(O_2)OOO(O_2)SF and FC(O)OOO(O_2)SF Trioxides: A Theoretical Study. *Chem. Phys. Lett.* **2014**, *616*−*617*, 81−85.
(47) Tucceri, M. E.; Badenes, M. P.; Bracco, L. L. B.; Cobos, C. J. Thermal Decomposition of 3-Bromopropene. A Theoretical Kinetic Investigation. *J. Phys. Chem. A* **2016**, *120*, 2285−2294.
(48) Phillips, L. F. Collision-Theory Calculations of Rate Constants for Some Atmospheric Radical Reactions over the Temperature Range 10−600 K. *J. Phys. Chem.* **1990**, *94*, 7482−7487.
(49) Powell, F. X.; Lide, D. R., Jr. Improved Measurement of the Electric-Dipole Moment of the Hydroxyl Radical. *J. Chem. Phys.* **1965**, *42*, 4201−4202.
(50) Saito, S.; Matsumura, C. Dipole Moment of the HO, Radical from Its Microwave Spectrum. *J. Mol. Spectrosc.* **1980**, *80*, 34−40.
(51) Reid, R. C.; Prausnitz, J. M.; Sherwood, T. K. *The Properties of Gases and Liquids*, 3rd ed.; MacGraw-Hill: New York, 1977.
(52) Hippler, H.; Troe, J.; Wendelken, H. J. Collisional Deactivation of Vibrationally Highly Excited Polyatomic Molecules. II. Direct Observations for Excited Toluene. *J. Chem. Phys.* **1983**, *78*, 6709−6717.
(53) Keyser, L. F. Kinetics of the Reaction OH + HO_2 → H_2O + O_2 from 254 to 382 K. *J. Phys. Chem.* **1988**, *92*, 1193−1200.
(54) Keyser, L. F. Absolute Rate Constant of the Reaction OH + HO_2 → H_2O + O_2. *J. Phys. Chem.* **1981**, *85*, 3667−3673.
(55) Dransfeld, P.; Wagner, H. G. Comparative Study of the Reactions of ^{16}OH and ^{18}OH with H$^{16}O_2$. *Z. Naturforsch. A* **1987**, *42a*, 471−476.
(56) Keyser, L. F.; Choo, K. Y.; Leu, M. T. Yields of O_2(b $^1\Sigma_g^+$) from Reactions of HO_2. *Int. J. Chem. Kinet.* **1985**, *17*, 1169−1185.

DOI: 10.1021/acs.jpca.6b10427
J. Phys. Chem. A 2017, 121, 440−447